IEEE Access
Multidisciplinary | Rapid Review | Open Access Journal

Received March 8, 2018, accepted April 5, 2018, date of publication April 16, 2018, date of current version May 2, 2018.

Digital Object Identifier 10.1109/ACCESS.2018.2826520

High-Speed Image Velocimetry System for Rainfall Measurement

CHIH-YEN CHEN[1], (Member, IEEE), CHI-WEN HSIEH[2], PO-WEI CHI[2], CHUN-FU LIN[1], CHUN-JEN WENG[1], AND CHI-HUNG HWANG[1], (Senior Member, IEEE)

[1]Instrument Technology Research Center, National Applied Research Laboratories, Hsinchu 30076, Taiwan
[2]Electrical Engineering Department, National Chiayi University, Chiayi City 60004, Taiwan

Corresponding author: Chi-Wen Hsieh (chiwen@mail.ncyu.edu.tw)

This work was supported by the Ministry of Science and Technology of Taiwan, R.O.C., under Grant MOST 103-2221-E-492-025 and Grant MOST 104-2221-E-492-038.

ABSTRACT In this paper, a new image-based disdrometer is developed to survey the movement of free falling raindrops. The proposed high-speed image velocimetry (HSIV) system comprises a high-speed camera mounted on a lens with long depth of field, a backlight source using an array of blue LEDs, and a computation/control unit for image acquisition and analysis. Further image processing algorithms are produced for raindrop detection and raindrop tracking. The performance of the HSIV system is compared with that of a commercial PARSIVEL^2 disdrometer during a local rainfall event within 12 h, while a tipping-bucket rain gauge is also used to estimate the amount rainfall rate during that period. The data obtained from the proposed HSIV system are in good agreement with those of PARSIVEL^2. Furthermore, the results of the HSIV system are closer than those of PARSIVEL^2 to the actual rainfall, which is determined by the rain gauge. To validate the raindrop tracking algorithm, another experiment is conducted to compare the tracking results with the frame-by-frame visual observation from 2880 consecutive frames within 5 min. Experimental results suggest that the proposed HSIV system facilitates the measurement of the precipitation properties, fall velocity, equivolume diameter, raindrop concentration, and rainfall rate, to real-time monitoring of the rainfall with stable and reliable analysis.

INDEX TERMS Rainfall rate, precipitation, raindrop size distribution, disdrometer, particle tracking.

I. INTRODUCTION

This measurement of precipitation is of crucial importance for meteorology, hydrology, and agriculture. Until now, rain gauge is the first device used to estimate precipitation by multiplying rainfall intensity by its duration. However, these devices cannot measure the microphysical properties of raindrops, which are crucial to the calibration of weather radar systems used to derive highly accurate estimates of precipitation [1].

Disdrometers use a variety of physical and mechanical principles to measure rainfall events [2]–[4]. Like the Joss–Waldvogel disdrometer (JWD), it employs the kinetic energy of free-falling raindrops to assess raindrop size distribution (RSD); however, the lack of raindrops' shapes makes it unable to provide detail precipitation properties [5]. Throughout the last half century, the radar-based microwave technology has been gradually surveyed and now become the most useful tool. Its principle is that radar system transmits microwaves in short pulses, and then measures the backscattering microwaves from raindrops with a short delay. Because the radar beams can travel long distances to detect the targets without any blockage, and such approach is particularly suitable for large scale observation of precipitation. The only weakness is that the radar observation depends substantially on ground precipitation to overcome poor spatial and/or temporal resolution [6].

Optical sensing techniques have been developed for use in hydrometers for the past two decades. In 2000, Löffler-Mang *et al.* [7] developed the particle size velocity (PARSIVEL) disdrometer, which uses a sensor to captures images of raindrops passing through a light beam to reconstruct the shape and compute the velocity of the raindrops. This method was expanded to produce a two-dimensional video disdrometer (2DVD), which can be used to derive the overall behavior of raindrops as well as their volume. In 2DVD, two orthogonal high-speed cameras were

employed to directly estimate the volume and velocity of raindrops; however, the high cost and complexity of these devices restrict their application in outdoor environments.

The hydrometeor velocity and shape detector (HVSD) was developed using two horizontally-situated parallel light beams separated vertically by 10 mm. Then, two line-scan cameras were respectively placed along the upper and lower planes to calculate the properties of free-falling raindrops [8]. Liu *et al.* [9] developed the CCD-based video precipitation sensor (VPS) with an external trigger to produce double exposures for the detection of falling raindrops. VPS is able to capture raindrops from images to measure the shape and velocity of raindrops. In [10], the authors developed a high-speed optical disdrometer (HOD) for measuring rainfall microphysical quantities. HOD can be combined with sensor-based methodologies for the observation volume around the focal plane to provide comprehensive data pertaining to raindrop characteristics. All these methods have inherent limitations with regard to measurement accuracy and robustness in field operations.

In this paper, a high-speed image velocimetry (HSIV) system is developed to automatically measure rainfall microphysics accurately during a rainfall event. Then, consecutive frames captured by a high-speed camera are used to isolate free-falling raindrops to estimate their shape, size, position, and fall velocity in order to derive the rainfall rate, accumulated rainfall, rainfall intensity, and RSD. The data are valuable for atmospheric research and weather forecasting. The remainder of this study includes descriptions of the components of the proposed HSIV system, the detection and processing of raindrop images, raindrop tracking to estimate precipitation, and the results of outdoor field tests.

II. PROPOSED HIGH-SPEED IMAGE VELOCIMETRY SYSTEM

With the aim of characterizing raindrops, the identification of each free-falling raindrop in different frames was conducted to analyze the movement of the raindrops in a short period. In the following, our experiment structure and the approaches of raindrop detection and raindrop tracking are described.

As shown in Fig. 1, the structure of the HSIV system comprises three main parts: a CMOS based high-speed camera (Basler acA640-750gm) with a lens, an array of blue LEDs as a backlight source, and a computation/control unit. High-speed images were captured at 500 frames per second, the exposure time of 69 μs, with a field of view covering 640 pixels $\times$ 480 pixels (with sensor size of 3.1 mm $\times$ 2.3 mm). To keep the sizes of the images constant, a specialized lens with a long working distance of 226 mm and extended depth of field of 192 mm was employed. To avoid distortion as possible, the focal distance was set to 120 mm, which is well within the depth of field. An LED backlight source (460 nm, Viswell, HBL-100) with a diffuser was used to create flat and uniform light. This illumination ensured that the raindrops were transparent and gave them distinctive edges to facilitate detection. All the specifications are listed in Table I.

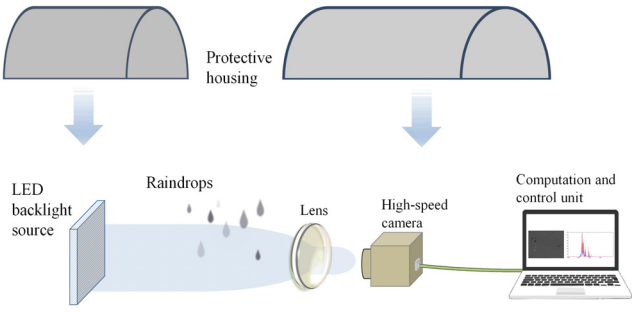

FIGURE 1. Experiment setup of the proposed HSIV system.

TABLE 1. Specifications of the system design.

Characteristics and units	Settings
Illumination light (nm)	460
Field of view (pixels × pixels)	640 × 480
Sensor size (mm × mm)	3.1 × 2.3
Imaging resolution (μm)	82
Acquisition frame (Hz)	500
Exposure time (μs)	69
Working distance (mm)	226
Depth of field (mm)	120

The control and computation unit performs two functions: data acquisition and image processing. Retrieved images were saved in PNG format with a filename corresponding to the date and specific time of capture. The high-speed camera was connected to a laptop computer via USB 3.0 for data transmission. The backlight source and the high-speed camera were sheltered from the wind and rain by two tunnel-type protective housings.

III. PROPOSED HIGH-SPEED IMAGE VELOCIMETRY SYSTEM

A. RAINDROP DETECTION

The positions of raindrops were determined according to changes in light intensity in a number of consecutive frames. Image pre-processing procedures were conducted to eliminate the effects of noise and interference from raindrops, dust, and dirt on the lens, while correcting for non-homogeneity in the light source. The steps are described in the below:

1) A median filter with 3× 3 window was used for image smoothing.

2) A reference background was constructed by the average of 500 images captured from each second time period.

3) A background subtraction was performed for each of these 500 images, and from which variations can be subtracted.

4) A useful threshold method referred to as Renyi entropy [11], was employed to maximize the two gray-level distributions of the raindrops and background.

A flowchart of the raindrop detection process is listed in Fig. 2. In the following, a description of Renyi entropy was presented.

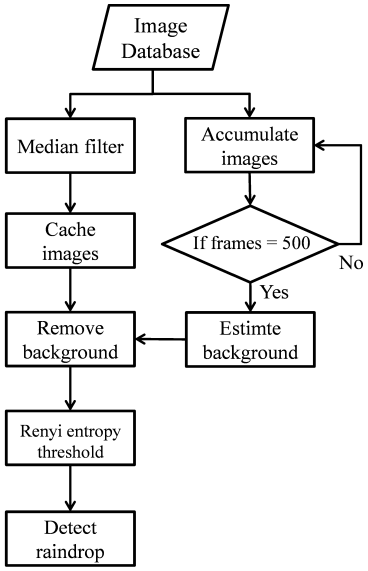

FIGURE 2. A flowchart of the raindrop detection algorithm.

For an $N \times M$ image, $f(x, y)$, the computation of Renyi entropy of order α is formulated as follows:

$$H_\alpha(P) = \frac{1}{1-\alpha} \ln \sum_{i=0}^{255} (p_i)^\alpha \tag{1}$$

where α is a positive real parameter not equal to 1, and p_i, $i = 0, 1, \cdots, k$ is the probability distribution of an image with k gray-levels. Then, with the use of a thresholding method, a gray-level image is usually divided into two distributions of object and background which are defined as follows:

$$\Lambda_1 : \frac{p_0}{P_1}, \frac{p_1}{P_1}, \cdots, \frac{p_t}{P_1}$$

and

$$\Lambda_2 : \frac{p_{t+1}}{P_2}, \frac{p_{t+2}}{P_2}, \cdots, \frac{p_k}{P_2}$$

where $P_1 = \sum_{i=0}^{t} p_i$, $P_2 = \sum_{i=t+1}^{k} p_i$, and $P_1 + P_2 = 1$.

Here, let k be 255, such that the Renyi entropy of order α is expressed as

$$H_\alpha^1(t) = \frac{1}{1-\alpha} \ln \sum_{k=0}^{t} \left(p_k/P_1\right)^\alpha \tag{2}$$

and

$$H_\alpha^2(t) = \frac{1}{1-\alpha} \ln \sum_{k=t+1}^{255} \left(p_i/P_2\right)^\alpha \tag{3}$$

$H_\alpha(t)$ is parametrically varied with respect to the threshold value, t. Then, the threshold value is considered to be optimized when the sum of (2) and (3) is maximized. The expression is formulated as:

$$t^*(\alpha) = Arg \max_{t \in G} \left[H_\alpha^1(t) + H_\alpha^2(t)\right] \tag{4}$$

These results are applied to the original image to produce a new image, as follows:

$$\begin{cases} f_t(x, y) = 0, & \text{if } f_t(x, y) \le t^*(\alpha) \\ f_t(x, y) = 1, & \text{otherwise} \end{cases} \tag{5}$$

We use α to adjust the threshold value, $t(\alpha)$ to obtain the optimal value.

To further evaluate the detection error of raindrop size, a test of using the HSIV system for measuring the glass balls of 1- to 5- mm diameters with 1 mm interval, was conducted to validate the processed images. The average errors for all the measurements of the glass balls are less than 6%. The maximum and minimum errors are in the groups of 1 and 5 mm glass ball with the errors of 5.3% and 2.1% respectively.

B. RAINDROP IDENTIFICATION FOR PAIR-MATCHING

The various particle tracking methods are categorized according to the representation of the target [12]–[15]. To observe the free-falling movement of raindrops, precipitation characteristics can be measured simply by assessing the shape, displacement, and orientation of the raindrops. Thus, accurately identifying the trajectory of raindrops frame-by-frame is crucial.

We represented raindrops as an ellipse and used the corresponding minimum bounding box as a replacement for the raindrops in calculating the equivolume diameter. The centroid calculated for the raindrop is the center of the bounding box. Let $\vec{r}_{ij}^{\,k}$ denote the displacement vector based on the following relationship:

$$\left|\vec{r}_{ij}^{\,k}\right| = \left|x_i^k - x_j^{k+1}\right|, \quad 1 \le i \le m,\ 1 \le j \le n, \tag{6}$$

where x_i and x_j are the positions of the i_{th} and j_{th} raindrop candidates in the k_{th} and $(k+1)_{th}$ frames, and m and n are the total number of detected raindrops in the k_{th} and $(k+1)_{th}$ frames.

The optimal pair-matching association of all raindrops in adjacent frames was obtained by calculating a cost for each individual trajectory of $\vec{r}_{ij}^{\,k}$ and the inverse $\vec{r}_{ji}^{\,k+1}$. The detail execution procedures were explained in the next section. Three important features, such as area difference, relative position, and oblateness variation, were used to evaluate the degree of similarity among raindrops and eliminate unwanted raindrop candidates. Additionally, some points related to features should be noted in the calculation as below. First, an assumption was made that the size of individual raindrops should not differ appreciably from frame to frame. Second, the desire of relative position of a given raindrop in the continuous frames was needed to be closed to the predicted value that was measured by multiplying the fall velocity of the

raindrop by the multiplicative inverse of the frame rate. Third, for the oblateness variation, it is clear that the oblateness of a raindrop is keeping similar within a short period.

Any raindrop can be assigned to more than one trajectory, and pair-matching is calculated frame by frame to determine the optimal cost of each. Our algorithm used to link raindrops from only two frames is based on an iterative estimation of match probability (Pro_{ij}) and no-match probability (Pro_i^*). Pro_{ij} is defined as the probability of matching each point x_j^{k+1} to a given point x_i^k, and Pro_i^* represents the probability that point x_i^k does not have a match in the second frame. For each displacement vector, $\vec{r}_{ij}^{\,k}$, the total cost of each trajectory is defined as follows:

$$C_{ij} = a \cdot \mathrm{A}_{ij} + b \cdot L_{ij} + c \cdot O_{ij} \tag{7}$$

where A_{ij}, L_{ij} and O_{ij} are the area difference, relative position, and oblateness variation respectively, and a, b and c are the assigned weights through the iterative experiment. Fig. 3 presents the flowchart of the raindrop tracking algorithm.

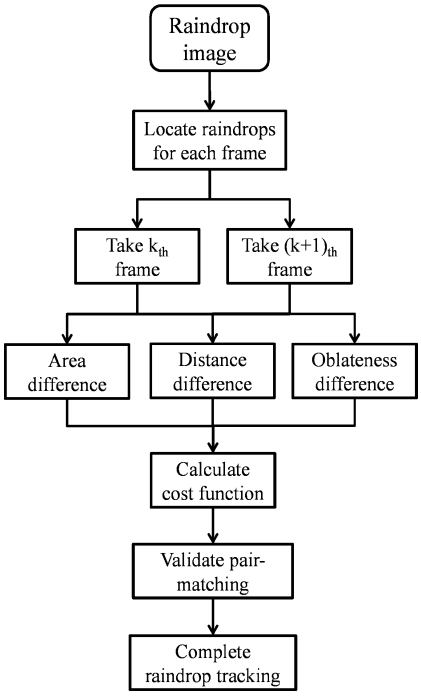

FIGURE 3. A flowchart of raindrop tracking algorithm.

C. COMPARISON OF THE PROPOSED HSIV SYSTEM WITH PARSIVEL²

The importance of using a variety of instrument to identify discrepancies in rainfall estimates has previously been reported. Thus, we used the second generation PARSIVEL² to evaluate the HSIV system with regard to rainfall rate and RSD. Subsequently, measurements of rainfall intensity were obtained at intervals of 1 min, and the performance of the disdrometers was presented minute by minute. A tipping-bucket rain gauge with resolution of 1 mm was used as a gold standard by which to evaluate the other measurements.

IV. RAINFALL MEASUREMENT AND DISCUSSION

The HSIV system was used to record rainfall events by obtaining images during the 1st second of consecutive 30-s periods. Image processing for raindrop detection and raindrop tracking were automatically applied to every frame. Captured frames were averaged over each 1-s interval to provide a reference background in order to make the raindrops stand out.

Renyi entropy thresholding was then applied to every captured frame for raindrop detection. Due to limited memory, we saved only the frames in which detected raindrops are combined. Only the frames in which each raindrop exceeds 5 pixels were left for further estimations. Furthermore, a calibration test was applied to the different sizes of the glass balls for evaluating the effectiveness of the HSIV system, and the results demonstrate that the errors are in a small range. The measurement error could be further improved by using stronger light source and higher resolution camera.

The movement of the free-falling raindrops was evaluated by computing a sequence of consecutive frames, in a process referred to as pair-matching aimed at linking two identical raindrops in the current and subsequent frames. This makes it possible to estimate the fall velocity of the raindrops according to their relative positions in two consecutive images. The total cost of the two trajectories, $\vec{r}_{ij}^{\,k}$ and $\vec{r}_{ji}^{\,k+1}$, whether it is C_{ij} or C_{ji}, can be computed based on pair-matching estimation of the i_{th} and j_{th} candidate raindrops in the k_{th} and $(k+1)_{th}$ frames. Only when C_{ij} and C_{ji} both present the highest probability is a pair-matching association identified for the trajectories of $\vec{r}_{ij}^{\,k}$ and the inverse $\vec{r}_{ji}^{\,k+1}$, which indicates the i_{th} raindrop moving to the position as j_{th} raindrop appeared in the frame. The i_{th} and j_{th} raindrops are then removed from the candidate pool, and the remaining raindrops are continuing to be evaluated. This process is repeated iteratively until no other raindrops can be linked.

Outdoor field test of the HSIV system has been performed during a rainfall event in Hsinchu, Taiwan, from 00:00 to 12:00 on 16 June, 2017 (UTC). After applying the filtering procedure, 73,928 frames from a total of 720,000 captured frames underwent analysis. Fig. 4 presents a sequence of 4 frames illustrating the performance of the proposed system with regard to raindrop detection and raindrop tracking. The green contours indicate the position of raindrops in the following frames. The relative positions of all raindrops passing through the sensing regions were detected in adjacent frames through the evaluation of all cost functions, from which are derived the optimal trajectories. The blue lines in the images indicate the pair-matching results.

To further verify the effectiveness of the method, the raindrop tracking algorithm based on the judgment of the authors was performed. The trajectories were visually examined frame by frame and then tagged as success or failure. The judge's criteria involved in identifying the trajectory of

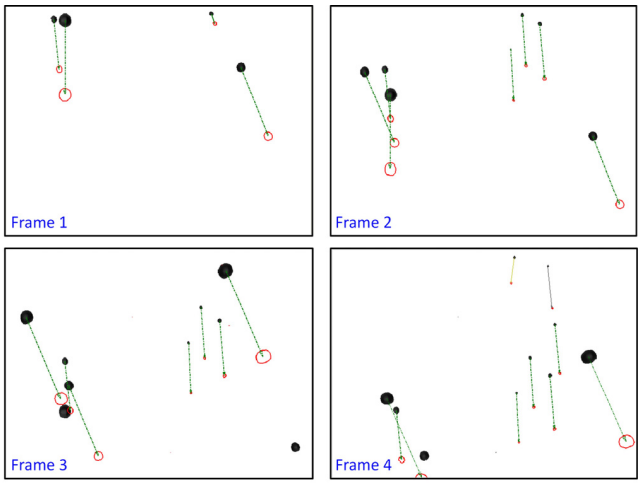

FIGURE 4. Application of raindrop tracking algorithm for a sequence of 4 grabbing frames.

a raindrop are including the area, shape and moving distance for the raindrop. We manually counted the number of raindrops in selecting 2880 consecutive frames, with respect to the maximum rainfall intensity from 02:11 to 02:15, for use as a reference in evaluating the accuracy of the system. The results of which are presented in Table II. In the verification experiment, 92.27 % raindrops were paired and only 7.72% raindrops were unpaired. Except for the unpaired raindrops, 85.95% of the pair-matching trajectories were successfully linked. Tracking errors may be due to the overlap of too many small raindrops in areas where raindrops formed dense collections. It should be emphasized that though there is a certain failure rate of the pair-matching trajectories during the maximum rainfall intensity, the influence on the measurement of rainfall rate is so small as to be unnoticeable. The reason is that the occurrence of the large amount and dense raindrops is low and the accumulation of these small raindrops is rather limited. These difficulties could be overcome by building up more robust raindrop detection and raindrop tracking algorithms in the future work.

TABLE 2. Evaluation of pair-matching trajectory from 02:11 to 02:15

Symbol	Success	Failure	Unlinked
Raindrops	667	109	65
Rate	85.95%	14.05%	×

After recording the RSD and rainfall rate over a period of 12 hrs, we calculated the total rainfall and minute-by-minute intensity (see appendix). Figures 5(a) and (b) respectively present the distributions of fall velocity and equivolume diameter (D_{eq}) over the study period using the HSIV system and PARSIVEL^2. Considering the influences of the measurement variation in different spaces [16]–[18], both of the two

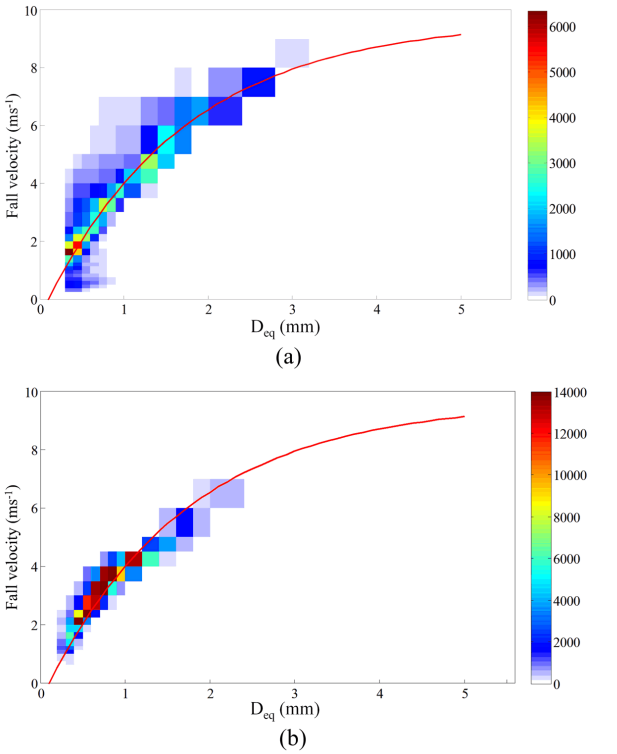

FIGURE 5. Distributions of fall velocity and equivolume dimeter by using the (a) HSIV system and (b) PARSIVE2 respectively.

disdrometers are placed in the same area within 1.5 meter apart to maintain as much consistency between spatial factor as possible. Overall, the RSD from both methods are similar to the empirical velocity relationship followed by Atlas *et al.* (1973) [19]. Our results revealed that 95% of the raindrops were of small diameter (0.5 m to 2 m), which is in good agreement with the results of PARSIVEL^2. Furthermore, a recent research has reported that the smaller raindrops between 0 mm to 3 mm are having faster fall velocity than expected [20] and [21], and the larger raindrops ($D_{eq} > 3$ mm) are falling slower than terminal fall velocity [22]. This behavior is consistent with the RSD of Fig. 5 in the smaller raindrops for both the PARSIVEL^2 and the HSIV system, but could not be found in the larger raindrops because of the rare occurrence. The results obtained using HSIV system presented slightly greater variation than did those of PARSIVEL^2, due to the fact that the raindrop tracking algorithm tolerates wide variations in fall velocity. It is also possible that different raindrops of the similar size may have been misjudged. Further refinement of the processing algorithms and an increase in the frame rate could further enhance performance in measuring RSD and rainfall. As shown in Fig. 6, the rainfall rate measured using HSIV is highly correlated with that obtained using PARSIVEL^2, with a correlation coefficient of 0.879. The highest rainfall rate was measured at 2:14, as follows: HSIV (1.02 mm) and PARSIVEL^2(1.64 mm). Overall, PARSIVEL^2 measured a slightly higher rainfall rate than did HSIV.

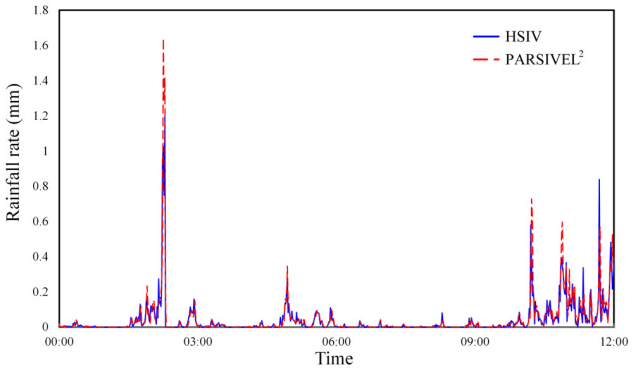

FIGURE 6. Rainfall rate over time as measured using HSIV and PARSIVEL^2.

The performance of the two systems was also evaluated according to the accumulated rainfall. As shown in Fig. 7, the results obtained using the HSIV system is in good agreement with the PARSIVEL^2 system, despite a number of random errors. Overall, the accumulated rainfall results obtained using HSIV and PARSIVEL^2 are consistent with those obtained using the rain gauge, as follows: HSIV (27.4 mm), PARSIVEL^2 (30.7 mm), and rain gauge (28.7 mm). We can notice that the HSIV results are close to those of the rain gauge, whereas the PARSIVEL^2 results are slightly higher. In the following, hourly rainfall accumulations from HSIV, PARSIVEL^2 and rain gauge are further analyzed. The result can be seen in Fig. 8 which shows the similar estimations and relatively small biases whether the rainfall rate is large or small. Next, the measurement of RSD using HSIV and PARSIVEL^2 are shown in Fig. 9. The blue curve presents the RSD obtained using HSIV whereas the red curve shows the RSD results obtained using PARSIVEL^2. Both curves present a similar trend in addition to the starting point of the equivolume diameter in 0.3 mm. This can be explained by the detection limit of the proposed system, and a higher resolution camera is enabling to improve it. As a whole, the RSD plots demonstrate the efficacy of the HSIV system in providing useful information pertaining to the constitution of raindrops for atmospheric research and weather forecasting.

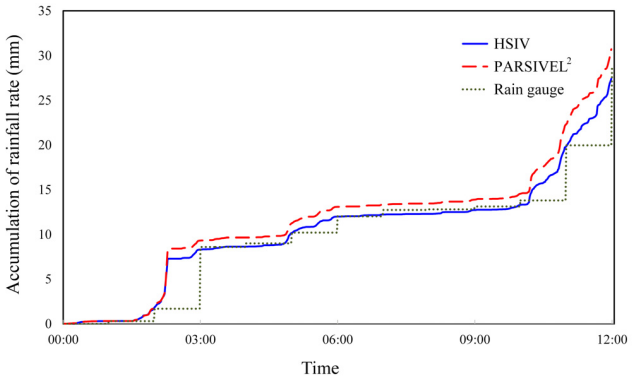

FIGURE 7. Accumulation of the rainfall as determined using HSIV, PARSIVEL^2 and rain gauge.

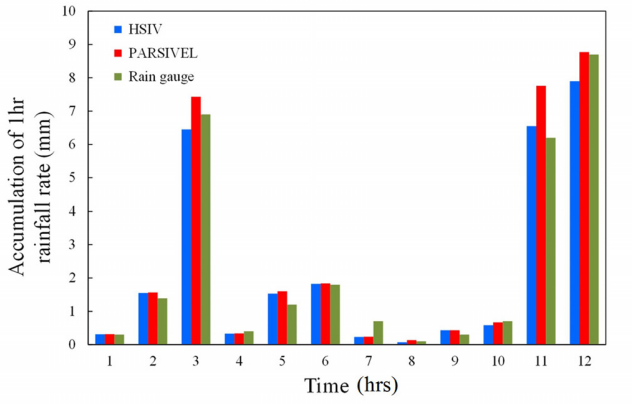

FIGURE 8. Accumulation of the 1hr rainfall accumulations from HSIV, PARSIVEL^2 and rain gauge.

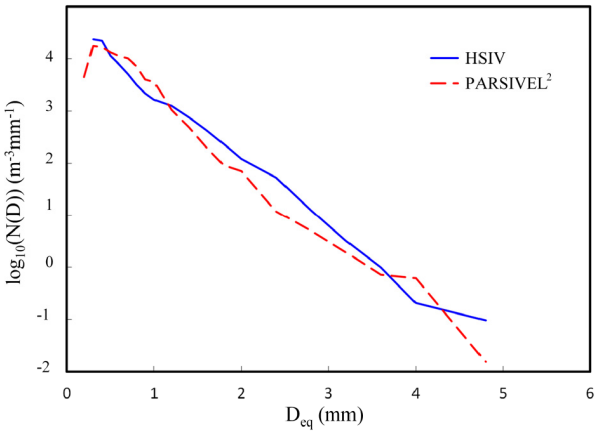

FIGURE 9. Measurement of RSD using HSIV and PARSIVEL^2.

According to the experiment results, the measuring trends between PARSIVEL^2 and HSIV system are generally in agreement with the rainfall rate over time, and their performances are within the studies scope. In the previous reports, some contradictories with respect to the estimation error from the PARSIVEL^2 are inevitable [23] and [24]. The conflicts can be considered as follows. First, the detecting raindrops of the PARSIVEL^2 technology are assumed to be ellipsoid and only one at once is passing through the sensing region toward the ground surface [7], [25]–[27]. Next, the estimation is susceptible to be influenced by turbulence and horizontal wind [22], [25], and [26]. The larger deviation angle of falling raindrops corresponds to the smaller fall velocity, and this is because of a reduced transit time. Third, a variety of sampling uncertainties, such as the splash contamination and margin raindrops without fully inside the sensing region, leads to the detection failures and increases the estimation errors [27] and [29].

All these factors can be attributed to the measuring mechanism of PARSIVEL^2 which employs a linear array of photodiodes to scan the falling particles and records each slice as it progresses through the sensing region. However, this

can be solved by using the proposed HSIV system despite the increase in complexity in raindrop detection and raindrop tracking. It should be noted that the aim of this study is not to belittle the PARSIVEL^2, but rather to focus on the new approach for assessing the movement of the free-falling raindrops by computing a sequence of consecutive frames captured from a high-speed camera and extracting the useful raindrops features for identifying each raindrop accurately. So, studies of the HSIV system is ongoing to further test and will be discussed to better understand its measuring limitations under different precipitation conditions.

V. CONCLUSION

This paper has described a novel scheme for the characterization of rainfall based on optical projections and image processing algorithms. Specifically, the methods for raindrop detection and raindrop tracking from captured images have been developed. Previous methods depend on manual settings to observe the movement of free-falling raindrops, whereas the proposed method is fully automated to provide data on the fall velocity, equivolume diameter, and concentration of raindrops, as well as the rate of rainfall.

The proposed HSIV system has been applied to a local rainfall event to measure the distributions of fall velocity and equivolume diameter, the accumulation of rainfall, and RSD. To evaluate the proposed system, PARSIVEL^2 and a tipping-bucket rain gauge were conducted for comparisons. The performance of HSIV system with regard to rainfall rate and RSD is in good agreement with those obtained using PARSIVEL^2. The difference between HSIV system and rain gauge measurements is smaller than that between PARSIVEL^2 and the rain gauge. Our results have demonstrated the efficacy of the HSIV system in the real-time monitoring of rainfall. Nonetheless, HSIV system falls short of PARSIVEL^2 with regard to variations in fall velocity distribution and equivolume diameter. In order to overcome these deficits, the proposed image processing algorithms will be tweaked to enhance pair-matching performance in the future.

APPENDIX

A. RAINFALL FEATURES

After detecting and identifying raindrops in two adjacent frames, the shape and the positions in each frame can be estimated to calculate all the related rainfall features.

1) FALL VELOCITY

Velocity of raindrop $\left|\vec{u}_{ij}^{k}\right|$ is calculated as follows:

$$\left|\vec{u}_{ij}^{k}\right| = \left|\vec{r}_{ij}^{k}\right| \Big/ \Delta t \tag{A.1}$$

where Δt is the time interval of the sampling frame. Note that the movement of free-falling raindrops is assumed to be close to its terminal velocity.

2) EQUIVOLUME DIAMETER

Under the effects of air drag, the raindrops do not appear perfectly spherical. Thus, we applied the equivolume ellipsoid to compute the diameter of the raindrops as follows:

$$D_{eq} = \left(\frac{6V}{\pi}\right)^{1/3} = \left(l^2 s\right)^{1/3} \tag{A.2}$$

where V is the volume of the raindrop, and l and s respectively indicate the long and short axes of the bounding box.

3) RAINDROP CONCENTRATION AND RAINFALL RATE

RSD describes the relationship between the concentration of raindrop $N\left(D_{eq}\right)$ and the corresponding equivolume diameter. This is computed as the total raindrop concentration (N_T) divided by the sampling volume of, using the following expression:

$$N\left(D_{eq}\right) = \frac{N_T\left(D_{eq}\right)}{A_s dD_{eq}} \tag{A.3}$$

The rainfall rate (R) can be obtained by integrating $N\left(D_{eq}\right)$, the fall velocity of $u\left(D_{eq}\right)$, and the equivolume diameter of D_{eq} from minimum to maximum, as follows:

$$R = \frac{\pi}{6 \times 10^4} \int_0^{\infty} N\left(D_{eq}\right) D_{eq}^3 u\left(D_{eq}\right) dD_{eq} \tag{A.4}$$

REFERENCES

[1] J. A. Nystuen, "Relative performance of automatic rain gauges under different rainfall conditions," *J. Atmos. Ocean. Technol.*, vol. 16, no. 8, pp. 11–23, Aug. 1999.

[2] G. Kathiravelu, T. Lucke, and P. Nichols, "Rain drop measurement techniques: A review," *Water*, vol. 8, no. 1, p. 29, Jan. 2016.

[3] A. Tokay, A. Kruger, and W. F. Krajewski, "Comparison of drop size distribution measurements by impact and optical disdrometers," *J. Appl. Meteor.*, vol. 40, no. 11, pp. 2083–2097, Nov. 2001.

[4] C. Caracciolo, R. Uijlenhoet, and F. Prodi, "Comparison between Pludix and impact/optical disdrometers during rainfall measurement campaigns," *Atoms. Res.*, vol. 82, nos. 1–2, pp. 137–163, Nov. 2006.

[5] J. Joss and A. Waldvogel, "Ein Spektrograph für Niederschlagstropfen mit automatischer Auswertung," *Pure Appl. Geophys.*, vol. 68, no. 1, pp. 240–246, Dec. 1967.

[6] A. Tassa, S. Di Michele, A. Mugnai, F. S. Marzano, and J. P. V. P. Baptista, "Cloud modelŰbased Bayesian technique for precipitation profile retrieval from the tropical rainfall measuring mission microwave imager," *Radio Sci.*, vol. 38, no. 4, p. 8074, Jun. 2003.

[7] M. Löffler-Mang and J. Joss, "An optical disdrometer for measuring size and velocity of hydrometeors," *J. Atmos. Ocean. Technol.*, vol. 17, no. 2, pp. 130–139, 2000.

[8] F. Y. Testik and M. K. Rahman, "High-speed optical disdrometer for rainfall microphysical observations," *J. Atmos. Ocean. Tech.*, vol. 33, no. 2, pp. 231–243, Feb. 2016.

[9] X. C. Liu, T. C. Gao, and L. Liu, "A video precipitation sensor for imaging and velocimetry of hydrometeors," *Atmos. Meas. Techn.*, vol. 7, no. 7, pp. 2037–2046, 2014.

[10] T. H. Raupach and A. Berne, "Correction of raindrop size distributions measured by Parsivel disdrometers, using a two-dimensional video disdrometer as a reference," *Atmos. Meas. Tech.*, vol. 8, no. 1, pp. 343–365, Jan. 2015.

[11] P. C. Sahoo Wilkins and J. Yeager, "Threshold selection using Renyi's entropy," *Pattern Recognit.*, vol. 30, no. 1, pp. 71–84, Jan. 1997.

[12] S. J. Baek and S. J. Lee, "A new two-frame particle tracking algorithm using match probability," *Experim. Fluids*, vol. 22, no. 1, pp. 23–32, Nov. 1996.

[13] Y. Choo and B. Kang, "Extraction of sizes and velocities of spray droplets by optical imaging method," *KSME Int. J.*, vol. 18, no. 7, pp. 1236–1245, Jul. 2004.

[14] L. A. Zarrabeitia, F. Z. Qureshi, and D. A. Aruliah, "Stereo reconstruction of droplet flight trajectories," *IEEE Trans. Pattern Anal. Mach. Intell.*, vol. 37, no. 4, pp. 847–861, Apr. 2015.
[15] G. Alcan, M. Ghorbani, A. Kosar, and M. Unel, "A new visual tracking method for the analysis and characterization of jet flow," *Flow Meas. Instrum.*, vol. 51, pp. 55–67, Oct. 2016.
[16] A. R. Jameson, M. L. Larsen, and A. B. Kostinski, "Disdrometer network observations of finescale spatialŰtemporal clustering in rain," *J. Atmos. Sci.*, vol. 72, no. 4, pp. 1648–1666, Nov. 2014.
[17] A. R. Jameson, M. L. Larsen, and A. B. Kostinski, "On the variability of drop size distributions over areas," *J. Atmos. Sci.*, vol. 72, no. 4, pp. 1386–1397, Jan. 2015.
[18] A. R. Jameson, M. L. Larsen, and A. B. Kostinski, "An example of persistent microstructure in a long rain event," *J. Hydrometeorol.*, vol. 17, no. 6, pp. 1661–1673, Jun. 2016.
[19] D. Atlas, R. C. Srivastava, and R. S. Sekhon, "Doppler radar characteristics of precipitation at vertical incidence," *Rev. Geophys.*, vol. 11, no. 1, pp. 1–35, Feb. 1973.
[20] G. Montero-Martínez, A. B. Kostinski, R. A. Shaw, and F. García-García, "Do all raindrops fall at terminal speed?" *Geophys. Res. Lett.*, vol. 36, no. 11, pp. 1–4, Jun. 2009.
[21] M. L. Larsen, A. B. Kostinski, and A. R. Jameson, "Further evidence for superterminal raindrops," *Geophys. Res. Lett.*, vol. 41, no. 19, pp. 6914–6918, Oct. 2014.
[22] M. Thurai, V. N. Bringi, W. A. Petersen, and P. N. Gatlin, "Drop shapes and fall speeds in rain: Two contrasting examples," *J. Appl. Meteorol. Climatol.*, vol. 52, no. 11, pp. 2567–2581, Nov. 2013.
[23] A. Tokay, W. A. Petersen, P. Gatlin, and M. Wingo, "Comparison of raindrop size distribution measurements by collocated disdrometers," *J. Atmos. Ocean. Tech.*, vol. 30, no. 8, pp. 1672–1690, Aug. 2013.
[24] A. Tokay, D. B. Wolff, and W. A. Petersen, "Evaluation of the new version of the laser-optical disdrometer, OTT Parsivel2," *J. Atmos. Ocean. Tech.*, vol. 31, no. 6, pp. 1276–1288, Jun. 2014.
[25] K. Friedrich, S. Higgins, F. J. Masters, and C. R. Lopez, "Articulating and stationary PARSIVEL disdrometer measurements in conditions with strong winds and heavy rainfall," *J. Atmos. Ocean. Tech.*, vol. 30, no. 9, pp. 2063–2080, Sep. 2013.
[26] A. Battaglia, E. Rustemeier, A. Tokay, U. Blahak, and C. Simmer, "PARSIVEL snow observations: A critical assessment," *J. Atmos. Ocean. Tech.*, vol. 27, no. 2, pp. 333–344, Feb. 2010.
[27] W. F. Krajewski *et al.*, "DEVEX-disdrometer evaluation experiment: Basic results and implications for hydrologic studies," *Adv. Water Resour.*, vol. 29, no. 2, pp. 311–325, Feb. 2006.
[28] L. Wen, K. Zhao, G. Zhang, S. Liu, and G. Chen, " Impacts of instrument limitations on estimated raindrop size distribution, radar parameters, and model microphysics during Mei-Yu season in East China," *J. Atmos. Ocean. Tech.*, vol. 34, no. 5, pp. 1021–1037, May 2017.

CHIH-YEN CHEN (M'10) received the master's degree in physics from National Taiwan Normal University in 2003 and the Ph.D. degree in biomedical engineering from National Yang-Ming University, Taipei, Taiwan, in 2010. He is currently an Assistant Researcher with the Instrument Technology Research Center, National Applied Research Laboratories, Taiwan. His research interests include instrument development for pattern recognition, disaster instrument, and computer-aided diagnosis in medical imaging.

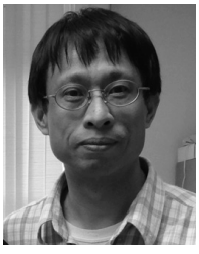

CHI-WEN HSIEH received the B.Sc. and Ph.D. degrees in electronic engineering from National Tsing-Hua University, Hsinchu, Taiwan, in 1993 and 2007, respectively. He has been an Associate Professor with the Department of Electrical Engineering, National Chiayi University, Taiwan, since 2009. His research interests include signal processing and medical electronics.

PO-WEI CHI was born in Tainan, Taiwan, in 1995. He is currently pursuing the master's degree in electrical engineering at National Chiayi University, Chiayi, Taiwan. His research interests include image processing and machine learning.

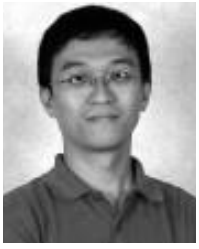

CHUN-FU LIN received the Ph.D. degree from the Institute of Electrical Control Engineering, National Chiao Tung University Taiwan, in 2014. Since 2010, he has been an Associate Researcher with National Applied Research Laboratories, Instrument Technology Research Center. His current research interests include image processing, image recognition, and intelligent system design.

CHUN-JEN WENG received the M.S. degree in electro-optical engineering from National Sun Yat-sen University in 2001 and the Ph.D. degree from the Department of Photonics, Institute of Electro-Optical Engineering, National Chiao Tung University in 2015. Since 2006, he has been an Associate Researcher with National Applied Research Laboratories, Instrument Technology Research Center, Taiwan. His research interests are in the area of microspectrophotometry, hyperspectral imaging, and tunable confocal laser system.

CHI-HUNG HWANG (M'09–SM'13) received the Ph.D. degree from the Department of Power Mechanical Engineering, National Tsing Hua University, Hsinchu, Taiwan, in 1996. He has been with the Instrument Technical Research Center as an Associated Research Fellow since 1996, where he is currently a Research Fellow and the Division Director. He is an AdCom-Members-at-Large of the IEEE Instrumentation and Measurement Society (2016–2019). He serves as a co-organizer of the 2017–2018 IEEE International Sensors and Measurement Student Contest.